Real-time method for the identification and quantification of hydrocarbon pyrolysis products: Part II. Application to transient pyrolysis and validation by numerical simulation

Nicolas Gascoin, G.A Abraham, Philippe Gillard, Marc Bouchez

Real-time method for the identification and quantification of hydrocarbon pyrolysis products: Part II. Application to transient pyrolysis and validation by numerical simulation.

Nicolas Gascoin[a1], Gregory Abraham[a], Philippe Gillard[a], Marc Bouchez[b]

[a]PRISME Institute, University of Orléans

63, avenue de Lattre de Tassigny, 18020 Bourges Cedex, France

[b]MBDA France

8, rue Le Brix, 18000 Bourges, France

Abstract

A real-time quantification Infra Red method has been developed with a gas cell to determine the composition of hydrocarbon pyrolysis products. The aim is to chemically characterise the fuel decomposition in case of regenerative cooling. The method can be extended to a large variety of applications. A transient analysis of the method behaviour is conducted to estimate its capacity to be applied to unsteady conditions (one measure per second), which can be encountered in cooling activity and unsteady processes. A numerical tool called RESPIRE (French acronym for Supersonic Combustion Ramjet Cooling with Endothermic Fuel, Transient Reactor Programming) is used to help understanding the complex phenomena involved in such a chemical reactor. The validation of transient behaviour with respect to the computations shows negligible time delay (lower than few seconds with gasification rate higher than 60 wt.%) due to residence time in the experimental setup. The quantification accuracy is confirmed to be around 2 mol.%. The agreement

[1] Corresponding author. Tel.: +33.248.238.473; fax: +33.248.238.871. *E-mail address:* Nicolas.Gascoin@bourges.univ-orleans.fr (N. Gascoin)

obtained on gas cell measurements is found to be correct over 10 wt% to 20 wt.% of gasification rate and very satisfactory over 60 wt.% but this depends on the species. An extension of the method has been developed with a dedicated online cell to be specifically applied to supercritical and multiphase flows. The quantification of the gas phase in the pyrolysis mixture in case of biphasic flow is proposed and validated with an uncertainty around 3 wt.%. The coke formation is monitored as a function of time and its quantification is even tested with 50 % of uncertainty after a numerical calibration with respect to simulation.

Keywords

Hydrocarbon pyrolysis; Fourier Transform Infra Red Spectrometer; Gas Chromatograph-Mass Spectrometer; supercritical state; kinetic simulation.

Nomenclature

GC: Gas Chromatograph

MS: Mass Spectrometer

HPLC: High Performance Liquid Chromatograph

FTIR: Fourier Transform Infra Red

CC: Combustion Chamber

CVI: Chemical Vapor Infiltration

CVD: Chemical Vapor Deposition

Ppm: part per million

1. Introduction

The hypersonic flight is expected to be achieved with Supersonic Combustion Ramjet engine [1]-[4]. Due to the large heat load applied on the structure (elevated total temperature in case of high speed [5],[6] and combustion heat release [7]), the regenerative cooling technique could be implemented to use the fuel as a coolant but also to voluntarily decompose it. Some of the resulting pyrolysis products (among hydrogen, ethylene, methane,… [8]) can

present sufficiently low auto-ignition delays for supersonic combustion conditions (auto-ignition delays should be 10 % of the residence time, that is to say 0.1 ms [9]). The COMPARER project (COntrol and Measure of PArameters in a REacting stReam) has been settled in 2003 to enable studying the regenerative cooling technique. To control such a technology, the combustion of the hydrocarbon pyrolysis products should be assessed and this requires estimating the main components and their respective concentrations [10]. For this purpose, a specific Infra Red method has been developed and validated under steady-state conditions [11]. Compared with Gas Chromatograph, it shows an accuracy of about 2 mol.% on the quantification of main gaseous products (detection limit of 4 mol.%) such as methane, ethylene, ethane, propylene and propane.

The aim of this second part of paper is to apply the method to transient cases to test its adaptability to conditions which are much more difficult to analyse. Due to its nature, the GC/MS apparatus is not suitable for transient analysis and the only way to validate the FTIR data is to use numerical simulation. For this purpose, the numerical code called RESPIRE (French acronym for SCRamjet Cooling with Endothermic Fuel, Transient Reactor Programming) uses experimental pressure, furnace temperatures and mass flow rate measurements as boundary conditions for an exact simulation of the pyrolysis process [7],[12]. This tool has been extensively validated since 2004 under various operating conditions, for several types of fluids, stationary and transient regimes [7].

1.1. Transient analysis of pyrolysis products formation

Very few studies are currently available on transient pyrolysis as it was already mentioned by Phuoc et al. [13] 20 years ago. Most of the "transient" studies are mainly numerically oriented in the sense that they aim at providing a kinetic mechanism which of course refers to the time [14]. Sprecher and Retcofsky [15] study the formation of free radicals whose lifetime is much lower than 1 ms (highly transient conditions) but they do it

after freezing the pyrolysis mixture (steady state conditions). Bauer [16] used this technique earlier with pyrolysed hydrocarbon fuels through shock-tube experiments. Lédé and coworkers [17] have conducted a kind of "transient" study but in fact they vary the pyrolysis time through successive experiments and analyse the products after the test and not during the test. Lacroix et al. [18] did the same for the formation of pyrocarbon. Consequently, no specific device is used but only common HPLC or MS apparatus. The work of Feron et al. [19] must be noticed because they used an FTIR spectrometer in situ to identify and quantify hydrocarbon and chlorous compounds directly inside the experiment. Nevertheless, they conducted the work under steady-state conditions to obtain stable reactor operation.

1.2. Reactive flow simulation

Due to the absence of experimental work related to transient estimation of pyrolysis and associated analytical techniques, the numerical simulation is an interesting tool for this study. The only transient studies related to pyrolysis are numerical ones because they are often coupled with combustion of products [20],[21]. Such computations are also found for catalysis [22] or CVI [23]. Despite their interest, they do not imply experimental validation in same unsteady conditions but at best under steady ones. It is even possible to find a work under "unsteady" conditions but which is in fact represented by stationary stages [24]. This approach is questionable since the transient phenomena are not a succession of stationary steps.

Several models of heat and mass transfer for fuel pyrolysis can be found. For active cooling applications, they consider different fuels and test configurations but few are related to transient analysis. They focus mainly on heat transfer, with limited consideration of the chemistry [25]-[29]. Most of the studies related to transient computations with detailed chemistry are related to combustion (with [30] or without pyrolysis [31],[32]) and very few are really dedicated to pyrolysis [33],[34].

2. The COMPARER test bench and the RESPIRE numerical code

2.1. Experimental apparatus

The COMPARER test bench has been fully described in [11]. It is representative of the SCRamjet engine. The fluid is heated and pyrolysed in the reactor by the oven, which represents the thermal effect of the combustion chamber. The test rig enables reaching a pyrolysis rate of 100 % for pressures up to 80 bar, temperatures up to at least 1200 K and mass flow rates lower than 0.6 $g.s^{-1}$. No fuel dilution is considered, which is sufficiently rare in pyrolysis studies to be mentioned. The bench has been predimensioned by the RESPIRE and NANCY tools [35] notably to get the same axial profiles in the reactor as in the cooling channel in terms of heat capacity, decomposition and Reynolds number but also to reach a similar outlet pyrolysis rate.

The pyrolysis products formed during experiments with isothermal plateaus have been monitored with respect to a large gas cell (volume of 100 cm^3, optical path length of 100 mm), which is placed approximately one meter after the outlet of the furnace (inner diameter of the line varies from 0.9 mm to 1.8 mm). This cell is kept at constant temperature of 373 K and its absolute pressure is regulated by a controlled vacuum pump at 50 mbar. The optical windows are in BaF_2 and a DTGS detector is used with this cell.

In addition to this large gas cell presented in a companion paper [11], another smaller one has been used with an MCT (Mercury Cadmium Telluride) detector cooled by liquid dinitrogen (outlet of the FTIR spectrometer) to increase the sensitivity and consequently the acquisition frequency (from one measure every 15 s to one per second). The cell (geometrical path length of 2 mm) is placed directly at the furnace outlet to obtain data on hot flows (depending on the unwanted natural cooling after the furnace). A scheme (Figure 1a) shows the IR signal path through the FTIR and the cell (Figure 1b). It must be noted that the cell is equipped with sapphire windows (no diamond window was available for this study) which do

not permit to measure the IR signal between 400 cm^{-1} and 1800 cm^{-1}. In comparison to the method presented in [11], it is much more difficult to provide a quantification method without this highly valuable signal range. So, studies performed with this cell have a less quantitative character; however, they provide interesting qualitative results, as will be seen later.

The main difference between the two optical cells is the volume and the path length which are smaller for the in-situ cell. Consequently, this latest shows a better dynamics which enables transient pyrolysis studies. Furthermore, the in-situ cell permits high pressure tests (60 bar at least) instead of controlling the absolute pressure around 50 mbar within the large gas cell. The temperature can reach 1000 K in the in-situ cell while it should be limited at temperature lower than 500 K in the large gas cell.

The acquisition parameters for this second configuration are the following:

- Number of scans for average: 1
- Optical resolution: 0.5 cm^{-1}
- Acquisition frequency: 1 Hz
- Acquisition range : 1600 cm^{-1} – 4000 cm^{-1}

Due to these changes and particularly to the optical windows, a new quantification method has been developed for this in situ cell (Table 1). Propane was the only species to be quantified in the range over 1800 cm^{-1} and this zone has not been kept because the other compounds are now searched in this area. The resulting determination factors are estimated with respect to calibrated mixtures. They are satisfactory for each species. The IR signal is linearly linked to the injected quantity. For each species, linear calibration curves have been obtained by least squares fitting using mixtures with known compositions. Satisfactory values of the determination factors have been obtained in all cases. Ethylene is not directly quantified. Its mole fraction is deduced from the sum of the other ones substracted to unity.

Figure 1 should be placed here

Table 1 should be placed here

2.2. Numerical tool

RESPIRE is a one dimensional transient compressible code with explicit Runge-Kutta 4th order time solving and finite difference 1st order upward scheme in space [9]. It uses semi-empirical correlations to account for laminar and turbulent regimes. The continuity, momentum and energy equations are solved to determine respectively density, velocity and temperature respectively [8]. The pressure is determined through an equation of state in which the compressibility factor takes the supercritical state particularities into account [8].

The fluid properties (heat capacity, thermal conductivity and dynamic viscosity) are computed for each species and mixture laws are applied to provide a single value for each position inside the reactor [12]. A detailed n-dodecane pyrolysis mechanism (1185 reactions, 153 species) is used [36] but any other mechanism can be taken as input. The species transport equations are solved using this mechanism as source terms.

A large effort has been done to validate the code with analytical, numerical and experimental data [9]. The heat transfers, the hydraulic and the chemistry have been studied with steady-state and transient cases for different fluid natures (mainly air, nitrogen and dodecane). Recently, computations with heptane, decane and kerosene have been conducted [7]. Actually, RESPIRE has been developed to represent the complete hypersonic vehicle with the combustion chamber, to compute the thrust and flight speed, and to enable the study of pyrolysis-combustion coupling [7],[9]. The code is also able to simulate the cooling channel alone, with either rectangular, pin fins or cylindrical geometry. This latest case is the one to be considered to simulate a chemical reactor with inner diameter of 4.35 mm.

The experimental measures of inlet pressure and mass flow rate but also those of temperatures in the furnace along the reactor (at least 6 measures) are used as boundary conditions during the same time which was necessary to conduct the experiments. As a consequence, the code allows obtaining the 1-D decomposition profile in the reactor, the

temperature distribution, all intermediate values such as the fluid properties, convective heat exchange coefficient or even mass flow rate which is not uniform due to compressibility effect. Other parameters can be calculated in a post-processing step, such as the residence time or the Reynolds number. To compare the data to experimental measurements, the composition at the process outlet only is considered in this paper, depending on the operating conditions, but a deeper study of pyrolysis phenomena is provided in [7].

3. Experimental and numerical pyrolysis results

Two series of experiments were carried out. In the first one (section 3.1), the experimental protocol is the same as in the first part of this paper [11]. We use a Titanium reactor with 4.5 mm inner diameter, n-dodecane as fuel, an ex-situ gas cell for FTIR measurements, as well as a GC/MS apparatus. The pressure and mass flow rate are fixed at 10 bar and 0.05 $g.s^{-1}$ respectively and five successive thermal steps are conducted generally by increasing the furnace temperature setup by 50 K or 100 K. The steps which do not present pyrolysis are not studied (from ambient to about 700 K depending on the operating conditions). The residence time is between 50 s and 150 s and a deeper analysis is given in [7],[9],[37]. It should be noticed that the reference temperature which is given in this study is the maximum value measured along the furnace length. No temperature sensor is available inside the chemical reactor. It has been shown in a previous study [9] that the maximum temperature reached by the fluid inside the process is very close to the maximum one in the oven (discrepancy lower than 30 K). Thus, this furnace temperature can be considered as a good indicator of temperature in the process itself. The second test series (section 3.2) will be detailed later and it uses an in-situ cell directly placed at the furnace outlet.

3.1. Data obtained with large gas cell (ex-situ FTIR setup) and temperature plateaus

The products to be considered in this section are only those quantified experimentally with

the gas cell presented in [11]. The mole fractions correspond to these species (CH_4, C_2H_4, C_2H_6, C_3H_6 and C_3H_8). The pyrolysis mixture compositions for each thermal steps obtained by GC/MS are listed in Table 2 (a first step was done at 823 K of furnace setup but no pyrolysis was detected either by GC/MS or FTIR). The pyrolysis rate increases over 50 wt.% for a maximum furnace temperature of 1055 K and the corresponding gasification rate is around 40 wt.%. This parameter is of great interest because it controls the filling of the gas cell, through the mass flow rate in the line. This is important for the dynamics of the FTIR measures. The numerical results are considered to be the reference because they are not impacted by transfer times after the process outlet.

In addition to the gas phase compounds, butane and pentane are found in major proportions in the liquid phase (Table 2). This distinction between the two phases depends on the ambient conditions which are: 1.01 bar and 295 K. Due to vapour pressure, some species found in liquid phase can also be evacuated for a negligible part in the gas phase. This has been estimated by an analytical computation and the butane content in the gas phase for example is of the order of few ppm to several tenth of ppm, which is judged negligible for the present work whose accuracy is more limited [11].

The production of methane during the pyrolysis stage rises with the fluid temperature through the furnace set point increase. The changes of temperature are indicated on Figure 2a with separation dashed lines to specify the beginning of set point increase for each thermal plateau. The numerical oscillations are attributed to computational instabilities and should not be interpreted as physical or chemical variations. The experimental oscillations are due to the quantification method during the post-processing and are also not physical. Large discrepancies are found between the computed and measured methane content for simulation times lower than 10000 s; that is to say for a furnace set point of 973 K (Figure 2a). This highlights a problem of gas cell filling due to its large volume (100 cm^3) in comparison to the

mass flow rate of gas phase. Indeed, an experimental gasification rate of 12 wt.% (Table 2) corresponds to a mass flow rate of 6 $mg.s^{-1}$ which is not entirely directed to the gas cell for safety reasons (99 % of the outlet flow goes to the burner). The flows directed to the GC/MS and to the FTIR are in similar proportions [37]. As a consequence, the mass flow in the FTIR is about 0.5 % of 6 $mg.s^{-1}$ (0.03 $mg.s^{-1}$). For an absolute pressure of 50 mbar, the cell needs 167 s to be filled entirely. This time is judged to be satisfactory and lower filling time is even better in case of higher gas production. For a furnace set point of 1023 K (numerical fluid temperature of 947 K), the accuracy is around 2 % as mentioned in [11] while at 1073 K (fluid temperature of 1020 K), the agreement is considered to be excellent (Figure 2a).

Table 2 should be placed here

For the 973 K plateau (experimental time from 9000 s to 16000 s on Figure 2a), the maximum fluid temperature to be reached is about 908 K and the corresponding gasification rate is 21 wt.% numerically. A value of 12 wt.% is found experimentally. The differences on this rate are mainly due to the numerical kinetic scheme. Indeed, the pyrolysis starts at 770 K numerically while negligible pyrolysis is experimentally observed for a furnace temperature of 864 K notably. This furnace temperature corresponds to a fluid temperature of 831 K (on the basis of simulation because no temperature sensor is available in the process). As a consequence, a thermal shift of about 50 K to 100 K is observed between the numerical scheme and the experiments. This was already observed previously [36]. This difference is reduced for higher temperature (for fluid temperature over 900 K).

For a maximum temperature measured in the furnace at 914 K (Table 2), the experimental gasification rate is around 7 wt.%. This corresponds to a filling time of the gas cell around 286 s. This gasification rate is judged to be the minimum one to obtain reasonable FTIR data. The regular increase of the experimental signal shows this cell filling (Figure 2a between 2500 s and 7500 s) and the slope could even be interpreted and be linked to the gasification

rate, through the mass flow rate provided to the gas cell line.

Some plateaus of ethylene mole fraction (Figure 2b) are clearly seen between 2500 s and 7500 s (temperatures up to 873 K). These ones should be considered carefully since the experimental method may not furnish reliable data for low gas production conditions. Indeed, even if only few ppm of gas are produced, they should be analyzed and a composition with a sum equal to unity should be found. This is not the case here for low gas production and this corresponds to the limitation of the method. It is mostly due to the dead volume of the bench and of the gas cell volume rather than to the FTIR technique or the quantification method itself. For gasification rate over 7 wt.% to 10 wt.%, the method starts to become reliable.

Figure 2 should be placed here

When the furnace temperature setup is increased from 823 K to 873 K (Figure 2b), the numerical ethylene content rises from 20 mol.% to 25 mol.% rapidly (gradient around 0.0177 mol.%.s^{-1}). This indicates a rapid and strong change in the operating conditions with a characteristic time around 100 s. This is attributed to the temperature sensitivity of the pyrolysis because it has been shown previously [9] that 100 % of pyrolysis can be obtained within a short thermal gradient of 50 K-100 K (typically for fluid temperature between 850 K and 950 K). As a consequence, changing the temperature by only 10 K in this range can modify significantly the pyrolysis and the gasification process. A regular ethylene content increase is observed numerically from 25 mol.% at 2500s to 27 mol.% at 5000 s while the temperature setup is not modified (gradient around 0.001 mol.%.s^{-1}). This is due to the stabilization time of heat transfer, which occurs principally by convection between the reactor wall and the fluid and is the limiting phenomenon involved in the bench (Figure 2c). A fluid temperature increase of 10 K is found between 3000 s and 4500 s of experimental time. These observations are also supported by the visualisations of the process itself through transparent tubes during the experiments. At the next change of set point temperature (from 873 K to

923 K) around 6200 s, the ethylene content increases suddenly from 27 mol.% to 30 mol.% (gradient of 0.018 mol.%.s^{-1}) for the same reason as for the preceding set point change.

Past the experimental time of 7500 s (numerical fluid temperature of 869 K and experimental gasification rate of 7 wt.%), the agreement between the RESPIRE code and the COMPARER bench results is satisfactory (maximum of 2 % of discrepancy).

Ethane formation is experimentally found to increase up to 7000 s of experiment before decreasing continuously while the numerical simulation shows in fact a constant decrease for the entire experimental time (Figure 3a). The limitation of the quantitative gas production is responsible for this discrepancy. Fundamentally, when gas formation appears, all of the five compounds (from CH_4 to C_3H_8) are produced. For the lowest temperature, ethane is one of the most important species in volume but propane and propylene are in majority in weight. After a temperature increase, propane and propylene are consumed to form lighter species. Thus, the absolute ethane content increases but its relative mole content decreases due to the formation of lighter methane. It is known that the ethane content can increase up to 1000 K at least before being consumed [9],[37]. Similar observations can be made for propylene formation (Figure 3b). The experimental IR signal for time lower than 7500 s is not reliable but a good agreement is found for gas production at higher times.

Figure 3 should be placed here

For gasification rate lower than 7 wt.% (time of 7500 s), the propane formation is not well measured while the simulation gives a maximum of 20 mol.% even if the total gas quantity represents a few ppm (Figure 4a). Because propane is the heaviest molecule to be quantified in the gas phase, its consumption can be observed for high temperature steps. This is clearly visible both experimentally and numerically for each temperature set point change (around 10100 s, 13600 s and 16100 s).

When the furnace temperature setup is increased to 973 K around 10100 s (Figure 4b), the

qualitative dynamics of the experiment is in good agreement with the numerical simulation with a time shift of 200 s. This time delay is reduced for higher gasification rate and it gets even negligible around 13600 s but still of the order of 100 s around 16100 s (Figure 4c and d). The agreement between RESPIRE and the IR measurements is accepted, despite of the discrepancy–up to 50 %-, because this represents around 2 mol.% in absolute quantity (Figure 4c and d). The detection limit of about 4 mol.% [11] is not visible for propane (Figure 4d).

For the change from 923 K to 973 K, the propane consumption gradient is about $-1.6.10^{-4}$ mol.%.s^{-1} experimentally and $-2.4.10^{-4}$ mol.%.s^{-1} numerically (Table 3). The relative difference is about 30 % between these two values but this remains quite reasonable because this causes a negligible difference in terms of propane mole content. These values are very low compared to preceding ones related to ethylene formation but they are judged to be significant because the maximum gradient found for stabilised temperature (between 7000 s and 10000 s) is $-2.7.10^{-5}$ mol.%.s^{-1} experimentally and $-4.5.10^{-5}$ mol.%.s^{-1} numerically. It is difficult to directly link the consumption gradient of propane to the temperature because no clear relationship appears (Table 3). This also depends notably on the nature and quantities of other compounds. Nevertheless, a higher consumption dynamics is shown for propane around 973 K to 1023 K of furnace setup (900 K to 950 K of fluid temperature) (Table 3).

Figure 4 should be placed here

Table 3 should be placed here

Thanks to the numerical approach, the dynamics of heat exchange and hydraulics can be observed (Figure 5a). The time needed by the furnace to reach the final temperature is about 140 s after the change of temperature setup while the fluid needs about 150 s and the pyrolysis rate about 280 s to stabilise. The chemistry is slower than heat transfer in this range of temperature because the initiation of pyrolysis (from 0.8 wt.% to 3.8 wt.%) is a slow phenomenon. It should increase very rapidly for higher rate due to exponential form of the

reaction equation (Arrhenius law). A negligible time delay is observed between the temperature increases of both furnace and fluid. However, a time delay of about 40 s is found between temperature and pyrolysis rate. This is of importance because it is impossible experimentally to observe such a delay (low gasification rate, high filling time of the gas cell).

For higher dodecane conversion (Figure 5b), the rise time of fluid temperature is about 120 s and some oscillations are visible due to stabilisation of the heating system. The one of fluid temperature and of pyrolysis are slightly higher (both about 140 s). The increases of fluid temperature and of pyrolysis rate show a time delay of 10 s and 20 s respectively after the furnace temperature rise. This is due to the exponential behaviour of the dodecane decomposition reaction (Arrhenius law), whose dynamics is very high. This is a good point for the FTIR because its measures are in better agreement with the calculations for high gasification rate. This shows that the present FTIR configuration is able to account for the transient changes to be encountered in the process at least with a characteristic time of 100 s. Due to the signal acquisition (one measure every 15 s [11]), it is probably the minimum time. The residence time remains relatively constant around 40 s because the density profile in the reactor is less sensitive to physical and chemical parameters than for lower temperature level.

Figure 5 should be placed here

To conclude this section, it must be noticed that the gas cell, as presented in [11], is limited due to its poor dynamics (cell size and transfer line) and to the relative content of gas species (instead of absolute quantity estimation). It is mainly suitable for sufficient gas production under steady-state conditions (fluid temperature higher than 900 K). For these reasons, another in situ cell has been used directly at the process outlet to cope with these first limitations and to get a transient analysis, including the liquid phase (next section).

3.2. Data obtained with in-situ cell under continuous heating

The in situ cell signal is more difficult to analyse because of the possible multiphase flow

during the pyrolysis (n-dodecane, 10 bar, 0.05 $g.s^{-1}$, Titanium reactor with inner diameter of 4.5 mm and thermal gradients of 10 $K.min^{-1}$ from 298 K to 1023 K). The raw spectrum displays a strong saturation due to the high liquid density. As a consequence, the in-situ cell reaches its limit even at "low" pressure. As a consequence, the IR signal in the range 2550 cm^{-1} - 3100 cm^{-1} is very difficult to analyse and it may even be unreliable to give quantitative results in this range at least under such low pyrolysis conditions. Other ranges of wavenumbers are polluted by atmospheric CO_2 and H_2O.

As a consequence, a zoom in the range 2400 cm^{-1}-3300 cm^{-1} is presented (Figure 6a). The transmission signal is given to limit the noise introduced after conversion in absorbance. Thus, the peak surface is computed for the part above the curve and not below as it would be done for absorbance signal. This surface decreases as a function of time with the temperature increase, which indicates that the liquid phase fraction diminishes. Accordingly, the gas phase quantity increases and the range 3000 cm^{-1}-3200 cm^{-1} presents characteristic peaks which are seen for the first time between 5159 s and 5161 s of experimental time. These pyrolysis initiations correspond to fluid temperature levels (e.g. 904 K at 5160 s) which are consistent with previous steady temperature studies (873 K-923 K as seen in Table 2).

Figure 6 should be placed here

The computed fluid temperature follows the furnace temperature during its increase and so does the pyrolysis rate (Figure 6b). For a furnace temperature around 910 K (Table 2), the fluid temperature was computed around 870 K in steady state while it is here in thermally transient conditions of 865 K. This discrepancy could be explained by the dynamics of transient heat exchange in the process but it is also low enough to estimate the stabilisation is reached for each time due to the low heating rate. As a consequence, using a thermal ramp (which is very well-known in other analysis tools such as Thermal Analysis) might be of interest to conduct pyrolysis studies instead of using steady state conditions because the

dynamics of the bench is shown to be fast enough with a heating rate of 10 K.min^{-1} to get almost stabilised conditions. However the time delay of 40 s observed between temperature and composition variations in the previous section could limit this point.

Furthermore, between all the curves given in Figure 6a, the maximum thermal discrepancy is about 13 K while the FTIR peak surface varies by more than a factor two. This does not correspond to the variation of pyrolysis rate because it only increases from 8 wt.% to 10 wt.% in the considered range (Figure 6b). Consequently, this may correspond to gas release due to some heterogeneous process (2-D effect in the reactor), to phase gliding between gas and liquid phases due to differential flow velocity, to phase separation due to gravity in the in situ cell for such a low speed flow or to gas formation increase due to the natural and unwanted cooling in the cell because of a lack in the thermal insulation. Due to the rapidity of the gas build-up (about 30 s) in large amounts (the liquid phase disappearance is related to the decrease of the upper peak surface), using a thermal transient gradient is difficult to get a fine analysis of the parameters, particularly if the IR acquisition frequency is not higher than 1 Hz.

The dynamics of the bench can be observed through the different experimental measurements (Figure 7). Around 5160s, the first gas signal is detected at the process outlet by the FTIR (while first gas formation is seen in the phase separator at 5255 s, downstream the FTIR cell) (Figure 7a). Around 5470 s, the fluid temperature measured in the in situ cell decreases instead of increasing with the furnace setup. This is attributed to a more important cooling of the pyrolysis mixture after the furnace and before the in situ cell (separated by about 5 cm of non insulated transfer line). This is reinforced by the mass flow rate decrease. Then due to pressure instabilities, the mass flow rate fluctuates strongly around 5600 s and after (Figure 7b). Due to amplification, the experiment was stopped at 6300 s. When the pressure overpasses the authorized limit, no mass flow is possible (6100 s), despite acquisition up to 6300 s. The data over 6100 s cannot be used for quantitative or qualitative exploitation.

Figure 7 should be placed here

The coking activity also participates to the thermal decrease observed in the in-situ cell because of its insulation effect [38]. For the Titanium reactor, coke has been shown not to be deposited in the reactor but to be formed in the main flow and to be evacuated toward the outlet. Thus, it should be detected by the FTIR. Indeed, the baseline of the IR signal is seen to be shifted toward high absorbance during the experiment but a tilt is also observable (Figure 8). This is due to the solid coke particles in the stream and this phenomenon has already been observed in literature [39]-[42]. Because no calibration has been done for the coke quantification, it is difficult to link quantitatively this signal change to the carbon deposit. Nevertheless, the coke formation is known to be related to acetylene and benzene production but also to methane because this highly hydrogenated compound compensates the hydrogen lack in the carbon deposit [38]. A preceding work on coking activity quantification [38] states that the mass of carbon deposit can be calculated by Eq. 1 where $A_{methane}$ .is the methane mole fraction integrated over the maximum furnace temperature (Eq. 1). A qualitative agreement is found between the tilt of the experimentally measured FTIR signal (which is seen on Figure 8) and the numerically estimated coke thickness through this quantification law (Figure 9). The following relationship could be proposed on the basis of this FTIR measure/numerical coke thickness relationship: $coke(cm) = {slope(cm)}/{coefficient}$ where the coefficient is proposed to be equal to 0.001 (dimensionless). This is a further step in the qualification of coke by using FTIR and a transient use is made possible. Nevertheless, this law gives an uncertainty of about 50 %.

$$m_{coke} = \frac{A_{methane} - 2096.3}{2193.7} \quad (1)$$

Figure 8 should be placed here

Figure 9 should be placed here

Another transient analysis of the FTIR signal would be of high interest for applied pyrolysis. The gas and liquid phases have been observed on the FTIR signal in the preceding section. Providing a quantification of both of them would allow giving the gasification rate. This rate can be linked to the pyrolysis rate and FTIR can indicate, as a result, the quantity of liquid n-dodecane. First of all, the gasification rate has been linked previously to the pyrolysis rate for n-dodecane with stainless steel [9] or Titanium [37] reactors, but also for other fluids [7]. The differences between the fluids are notably due to their nature and molecular weight. As a consequence, the gasification rate can be a good indicator of the pyrolysis stage. A preliminary approach of its transient quantification is proposed. Two zones are identified on the IR signal and are attributed to both phases (Figure 10a). The areas of these zones are computed as a function of time during the experiment. The ratio of both surfaces is then plotted as a function of experimental time (Figure 10b). The dot corresponds to experimental steady-state configurations [11] which are placed on a time scale with respect to the corresponding furnace temperature. Indeed, it has been mentioned earlier that only 5 K of discrepancy is numerically found on the fluid temperature between permanent and transient state. This justifies using the steady-state conditions for comparison. The same graph can also be proposed as a function of maximum measured oven temperature (Figure 10c). Finally, a reasonable agreement is found between both types of data. This validates the transient quantification of the gas phase, thus of the pyrolysis rate through relationship found previously [7].

Figure 10 should be placed here

An illustrative calculation has been done with NIST data on CH_4 and $C_{12}H_{26}$ IR spectra. The n-dodecane spectrum has been modified by addition of methane with different concentrations (molar fractions). For a zoom in on pure n-dodecane signal (Figure 11a), the addition of methane (2 mol.%) clearly modifies a thin interval of the spectrum around

3100 cm^{-1} (Figure 11b). When increasing the methane content, which is representative of gas formation whatever the chemical nature, the area which is judged to be representative of the gas phase (Figure 10a) increases through Figure 11c to Figure 11d. This also justifies trying to quantify the gas formation through the analysis of the IR spectrum in the wave number range of 3000 cm^{-1} - 3200 cm^{-1}.

Figure 11 should be placed here

4. Conclusions

Unsteady behaviour can be easily encountered in the pyrolysis of hydrocarbon fuels. A dedicated FTIR method has been presented and validated under steady-state conditions to identify and quantify the main pyrolysis products. The ability of the method to be applied to transient cases has been tested in this paper and compared to numerical simulations. A minimum gas production (around 7 wt.% to 10 wt.%) is required to get a satisfactory quantification of the gas phase by IR measurements on the sampling line. The large dead volume after the process outlet, the off-line gas cell volume and the mass flow rate in the transfer line are the restricting parameters which require high gasification rate to contend these limitations. The agreement between computed and measured mole fraction of gas compounds is found in a margin of 2 % even during transient variations, which is satisfactory. Two dynamic steps in the products formation are found when a temperature increase is applied to the furnace. The sudden higher gas formation is responsible for a first step whose gradient is quite high (around 0.018 mol.%.s^{-1}). Then a second step, whose dynamics is much lower (0.001 mol.%.s^{-1}), is attributed to the temperature stabilisation, mostly due to the conduction in the reactor. A time delay of up to 40 s between temperature and composition variations has been evidenced. This delay largely reduces with the temperature level.

In-situ measurements have been conducted under transient thermal heating with respect to

a dedicated in-situ cell directly at the pyrolysis process outlet. Diamond windows (instead of sapphire ones) would be of great interest for the quantification method. The dynamics of the bench is fast enough to follow the pyrolysis stage and coke formation. A coking alert has been established on the basis of transient FTIR data. A quantification of the gasification has been done with an accuracy of 3 %. As perspectives, the in-situ cell will be used in steady-state conditions with isothermal plateaus to compare data with those obtained with the large cell.

Acknowledgements

The present work has been carried out with the contribution of the "Conseil Général du Cher (18)", of Bourges Plus, of the FRED, of the FEDER, of the FSE (European Union Special Funding) and of MBDA-France. The good evolution of the COMPARER project was made possible thanks to the contribution of Y. Parmantier, who is in charge of the project and the coordinator of the "Pôle Capteurs et Automatismes" of Bourges.

References

[1] R.S. Fry, J. Prop. Power 20 (January–February (1)) (2004).

[2] C.R. McClinton, X-43 SCRamjet Power Breaks the Hypersonic Barrier Dryden Lectureship in Research for 2006. AIAA 2006; 1.

[3] E.H. Andrews, SCRamjet Development and Testing in the United States. AIAA 2001; 1927.

[4] E.T. Curran, SCRamjet Engines: The First Forty Years. Journal of Propulsion and Power 2001; Vol. 17, No. 6, pp. 1138–1148.

[5] M. Bouchez, S. Beyer, 13th Hypersonics Systems and Technologies Conference, 2005, AIAA-2005-3434.

[6] N. Gascoin, P. Gillard, S. Bernard, G. Abraham, M. Bouchez, E. Daniau, Y. Touré, 14th Hypersonic Systems and Technologies Conference, Canberra, Australia, 6–9 November, 2006, AIAA-2006-8005.

[7] N. Gascoin, G. Abraham, P. Gillard, J. Anal. Appl. Pyrol. 89 (2010) 294-306.

[8] N. Gascoin, P. Gillard, S. Bernard, E. Daniau, M. Bouchez, Pyrolysis of Supercritical Endothermic Fuel: Evaluation for Active Cooling Instrumentation, IJCRE, vol. 6, A7 ed., The Berkeley Electronic Press, 2008.

[9] N. Gascoin, Etude et mesure de paramètres pertinents dans un écoulement réactif application au refroidissement par endo-carburant d'un super-statoréacteur, Editions Universitaires Européennes, April 2010, ISBN13: 978-6131501074, p. 376.

[10] N. Gascoin, P. Gillard, M. Bouchez, 16th Hypersonic Systems and Technologies Conference, Bremen, Germany, 2009, AIAA-2009-7375.

[11] G. Abraham, N. Gascoin, P. Gillard, M. Bouchez, Real-time method for the identification and quantification of hydrocarbon pyrolysis products: Part I. Development and validation of the Infra Red technique., **JAAP, under submission for reviewing process.**

[12] N. Gascoin, P. Gillard, E. Dufour, Y. Touré, J. Thermophys. Heat Trans. 21 (January to March (1)) (2007) 86–94

[13] T.X. Phuoc, M.P. Mathur, Transient heating of coal particles undergoing pyrolysis, Combustion and Flame, Volume 85, Issues 3-4, June 1991, Pages 380-388.

[14] T.P. Griffin, J.B. Howard, W.A. Peters, Pressure and temperature effects in bituminous coal pyrolysis: experimental observations and a transient lumped-parameter model, Fuel, Volume 73, Issue 4, April 1994, Pages 591-601.

[15] R.F. Sprecher, H.L. Retcofsky, Observation of transient free radicals during coal pyrolysis, Fuel, Volume 62, Issue 4, April 1983, Pages 473-476.

[16] S.H. Bauer, Transient species generated during the pyrolysis of hydrocarbons, Symposium (International) on Combustion, Volume 11, Issue 1, 1967, Pages 105-115.

[17] J. Lede, F. Blanchard, O. Boutin, Radiant flash pyrolysis of cellulose pellets: products and mechanisms involved in transient and steady state conditions, Fuel, Volume 81, Issue 10, July 2002, Pages 1269-1279.

[18] R. Lacroix, R. Fournet, I. Ziegler-Devin, P.-M. Marquaire, Kinetic modeling of surface reactions involved in CVI, of pyrocarbon obtained by propane pyrolysis, Carbon, Vol. 48 (2010), pp 132 –144

[19] O. Feron, F. Langlais, R. Naslain, In-situ analysis of gas phase decomposition and kinetic study during carbon deposition from mixtures of carbon tetrachloride and methane, Carbon 37 (1999) 1355–1361

[20] M. M. Delichatsios, M. A. Delichatsios, Effects of transient pyrolysis on wind-assisted and upward flame spread, Combustion and Flame, Volume 89, Issue 1, April 1992, Pages 5-16.

[21] Y. Pizzo, J.L. Consalvi, B. Porterie, A transient pyrolysis model based on the B-number for gravity-assisted flame spread over thick PMMA slabs, Combustion and Flame, Volume 156, Issue 9, September 2009, Pages 1856-1859.

[22] A. Hinz, B. Nilsson, A. Andersson, Simulation of transients in heterogeneous catalysis: a comparison of the step- and pulse-transient techniques for the study of hydrocarbon oxidation on metal oxide catalysts, Chemical Engineering Science, Volume 55, Issue 20, 15 October 2000, Pages 4385-4397.

[23] A. Li, O. Deutschmann, Transient modeling of chemical vapor infiltration of methane using multi-step reaction and deposition models, Chemical Engineering Science, Volume 62, Issues 18-20, 19th International Symposium on Chemical Reaction Engineering - From Science to Innovative Engineering - ISCRE-19, September-October 2007, Pages 4976-4982.

[24] S. F. Son, M. Quinn Brewster, Unsteady combustion of homogeneous energetic solids using the laser-recoil method, Combustion and Flame, Volume 100, Issues 1-2, January 1995, Pages 283-291.

[25] T. Kanda Study of an Airframe-Integrated Scramjet Engine System, AIAA Paper 2000-3705, 2000.

[26] T. Kanda, G. Masuya, F. Ono, Y. Wakamatsu, Effect of Film Cooling/Regenerative Cooling on Scramjet Engine Performances, Journal of Propulsion and Power, Vol. 10, No. 5, Sept.–Oct. 1994, pp. 618–624.

[27] Y. Tsujikawa, G.B. Northam, Effects of Hydrogen Active Cooling on Scramjet Engine Performance, International Journal of Hydrogen Energy, Vol. 21, No. 4, 1996, pp. 299-304.

[28] T. Kanda, K. Kudo, Conceptual Study of a Combined-Cycle Engine for an Aerospace Plane, Journal of Propulsion and Power, Vol. 19, No. 5, Sept.–Oct. 2003, p. 6176.

[29] A.T. Wassel, F. Lssacci, V. Van Griethuysen, An Integrated Modelling Approach for Hypersonic Aircraft Thermal Management, AIAA Paper 1995-6022, 1995.

[30] L. Allancon, B. Porterie, J.C. Loraud, E. Daniel, Unsteady convection in a cavity due to pyrolysis, Mechanics Research Communications, Volume 20, Issue 2, March-April 1993, Pages 173-179.

[31] A. Cuoci, A. Frassoldati, T. Faravelli, E. Ranzi, Formation of soot and nitrogen oxides in unsteady counterflow diffusion flames, Combustion and Flame, Volume 156, Issue 10, October 2009, Pages 2010-2022.

[32] D. B. Bullard, L. Tang, R. A. Altenkirch, S. Bhattacharjee, Unsteady flame spread over solid fuels in microgravity, Advances in Space Research, Volume 13, Issue 7, July 1993, Pages 171-184.

[33] B. V. Babu, A. S. Chaurasia, Pyrolysis of biomass: improved models for simultaneous kinetics and transport of heat, mass and momentum, Energy Conversion and Management, Volume 45, Issues 9-10, June 2004, Pages 1297-1327.

[34] C. Di Blasi, Influences of model assumptions on the predictions of cellulose pyrolysis in the heat transfer controlled regime, Fuel, Volume 75, Issue 1, January 1996, Pages 58-66.

[35] N. Gascoin, P. Gillard, Y. Touré, S. Bernard, E. Daniau, M. Bouchez, Modélisation Hydraulique et Thermique d'un Fluide Supercritique avec Pyrolyse dans un Canal Chauffé:

Prédimensionnement d'une Etude Expérimentale Congrès Franc¸ ais de Thermique, SFT, Reims, France, 30 mai–2 juin, 2005.

[36] K.D. Dahm, P.S. Virk, R. Bounaceur, F. Battin-Leclerc, P.M.Marquaire, R. Fournet, E. Daniau, M. Bouchez, J. Anal. Appl. Pyrol. 71 (2004) 865–881.

[37] G. Abraham, Etude et développement d'une méthode d'analyse par spectroscopie infrarouge appliquée à la pyrolyse d'hydrocarbures en conditions supercritiques et transitoires, Ph.D. Thesis, December 2009, University of Orléans, France.

[38] N. Gascoin, P. Gillard, S. Bernard, M. Bouchez, Fuel Process Technol. 89 (December (12)) (2008) 1416–1428.

[39] K. Matsushita, A. Hauser, A. Marafi, R. Koide, A. Stanislaus, Initial coke deposition on hydrotreating catalysts. Part 1. Changes in coke properties as a function of time on stream, Fuel 83 (2004) 1031-1038

[40] A. Galvez, N. Herlin-Boime, C. Reynaud, C. Clinard, J.N. Rouzaud, Carbon nanoparticles from laser pyrolysis, Carbon 40 (2002) 2775-2789

[41] I. Llamas-Jansa, C. Jäger, H. Mutschke, Th. Henning, Far-ultraviolet to near-infrared optical properties of carbon nanoparticles produced by pulsed-laser pyrolysis of hydrocarbons and their relation with structural variations, Carbon 45 (2007) 1542-1557

[42] V. A. Maroni, S. J. Epperson, An in situ infrared spectroscopic investigation of the pyrolysis of ethylene glycol encapsulated in silica sodalite, Vibrationnal Spectroscopy 27 (2001) 43-51

Table 1. IR zones of quantification for both cells and determination factor of the in situ cell method.

	Gas cell [11] (cm^{-1})	In situ cell (cm^{-1})	Determination factor (in situ cell)
Methane	1300-1310	3161-3170	0.98711
Ethylene	1875-1910	-	-
Ethane	820-825 1529-1533	2700-2790	0.99758
Propylene	1640-1650	1766-1933	0.99927
Propane	2860-2890	3300-3380	0.99329

Table 2. GC/MS Mass fraction of n-dodecane pyrolysis products for five thermal plateaus (10 bar, 0.05 g.s^{-1}, Ti reactor).

	Maximum Measured Furnace temperature (K)				
	864	914	964	1009	1055
hydrogen (G)	0.00%	0.00%	0.00%	0.00%	0.00%
methane (G)	0.00%	0.79%	1.21%	2.45%	4.91%
acetylene (G)	0.00%	0.00%	0.00%	0.00%	0.00%
ethylene (G)	0.00%	2.23%	3.68%	7.06%	13.06%
ethane (G)	0.00%	1.67%	2.47%	4.08%	6.90%
propylene (G)	0.00%	1.56%	3.49%	6.96%	14.47%
propane (G)	0.00%	1.16%	1.36%	1.65%	1.65%
butene (G)	0.00%	0.00%	0.00%	0.00%	0.00%
butane (L+G)	0.00%	0.00%	0.00%	3.34%	4.80%
pentene (L+G)	0.00%	0.00%	0.00%	0.00%	0.00%
pentane (L+G)	0.00%	0.00%	0.00%	2.33%	3.00%
Cyclopentane (L)	0.00%	0.00%	0.00%	0.00%	0.00%
hexene (L+G)	0.10%	0.08%	0.06%	0.06%	0.06%
hexane (L+G)	0.08%	0.06%	0.05%	0.03%	0.04%
Benzene (L)	0.00%	0.00%	0.00%	0.00%	0.00%
Cyclohexane (L)	0.00%	0.00%	0.00%	0.00%	0.00%
Cyclohexene (L)	0.00%	0.00%	0.00%	0.00%	0.00%
heptene (L+G)	0.00%	0.00%	0.00%	0.00%	0.00%
heptane (L+G)	0.02%	0.02%	0.01%	0.01%	0.01%
octene (L+G)	0.00%	0.02%	0.02%	0.03%	0.06%
octane (L+G)	0.00%	0.00%	0.00%	0.00%	0.01%
toluene (L)	0.00%	0.00%	0.00%	0.00%	0.00%
p-xylene (L)	0.00%	0.00%	0.00%	0.00%	0.00%
ethylbenzene (L)	0.00%	0.00%	0.00%	0.00%	0.01%
nonene (L)	0.03%	0.13%	0.35%	0.34%	0.37%
nonane (L)	0.00%	0.00%	0.04%	0.04%	0.04%
decene (L)	0.05%	0.28%	1.33%	1.29%	1.42%
decane (L)	0.16%	0.14%	0.18%	0.14%	0.11%
undecene (L)	0.02%	0.12%	0.47%	0.43%	0.41%
undecane (L)	0.15%	0.14%	0.20%	0.14%	0.00%
dodecene (L)	0.00%	0.00%	0.09%	0.01%	0.00%
n-dodecane (L)	99.39%	91.61%	84.98%	69.61%	48.67%
tridecene (L)	0.00%	0.00%	0.00%	0.00%	0.00%
tridecane (L)	0.00%	0.00%	0.00%	0.00%	0.00%
tetradecene (L)	0.00%	0.00%	0.00%	0.00%	0.00%
tetradecane (L)	0.00%	0.00%	0.00%	0.00%	0.00%
Gasification rate	0.00%	7.40%	12.20%	22.20%	41.00%
Pyrolysis rate	0.61%	8.39%	15.02%	30.39%	51.33%

Table 3. Consumption gradients (mol.%.s^{-1}) of propane for successive thermal increases.

Furnace setup	923	973	1023	1073
Experiment	-	$-1.6.10^{-4}$	$-3.2.10^{-4}$	$-9.2.10^{-5}$
Simulation	$-1.2.10^{-4}$	$-2.4.10^{-4}$	$-2.32.10^{-4}$	$-1.2.10^{-4}$

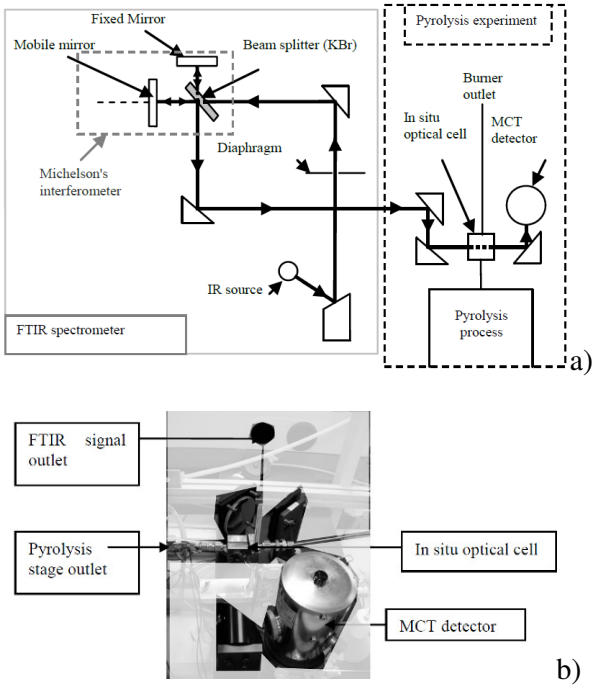

Figure 1. Path of the Infra Red signal from the FTIR source to the MCT detector (a) and related photograph with the in situ cell (b).

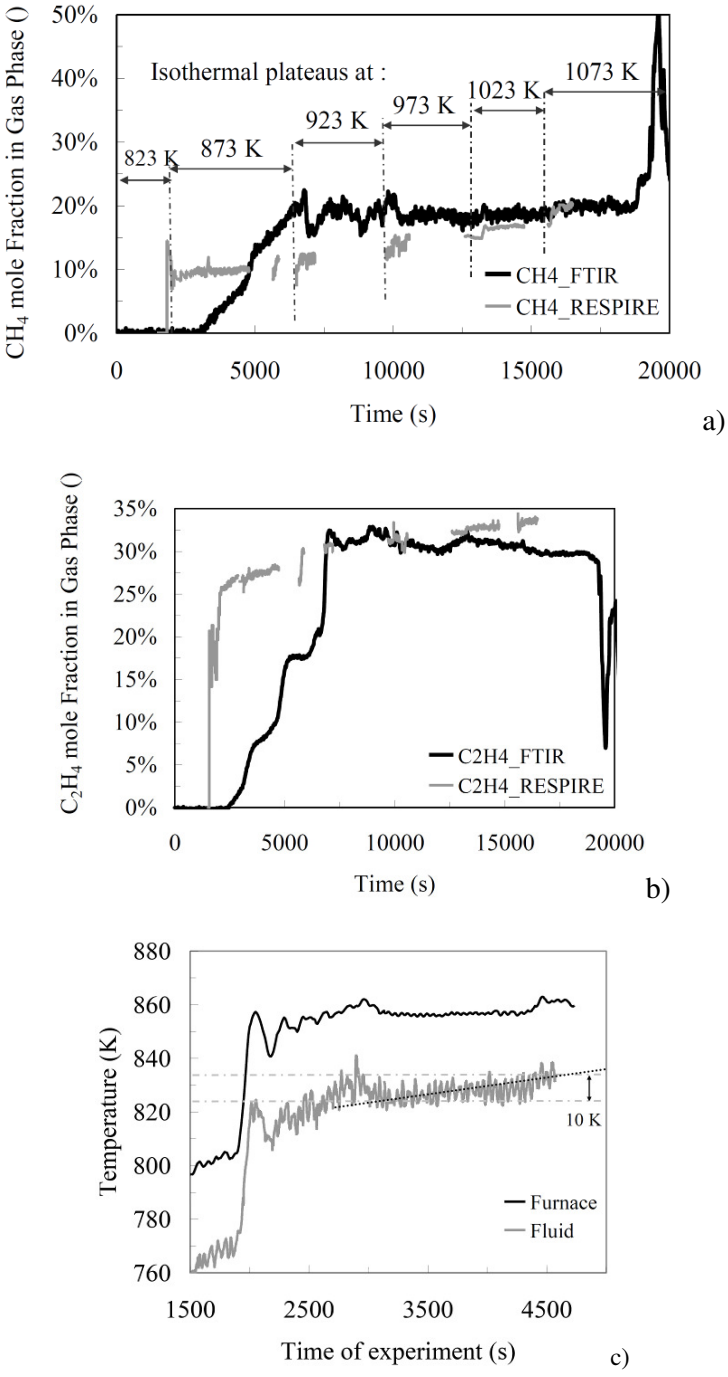

Figure 2. Measured and filtrated computed methane (a) and ethylene (b) mole fractions as a function of time for dodecane pyrolysis (10 bar, 0.05 g.s^{-1}, Ti reactor) with corresponding time history of fluid and furnace temperatures (c).

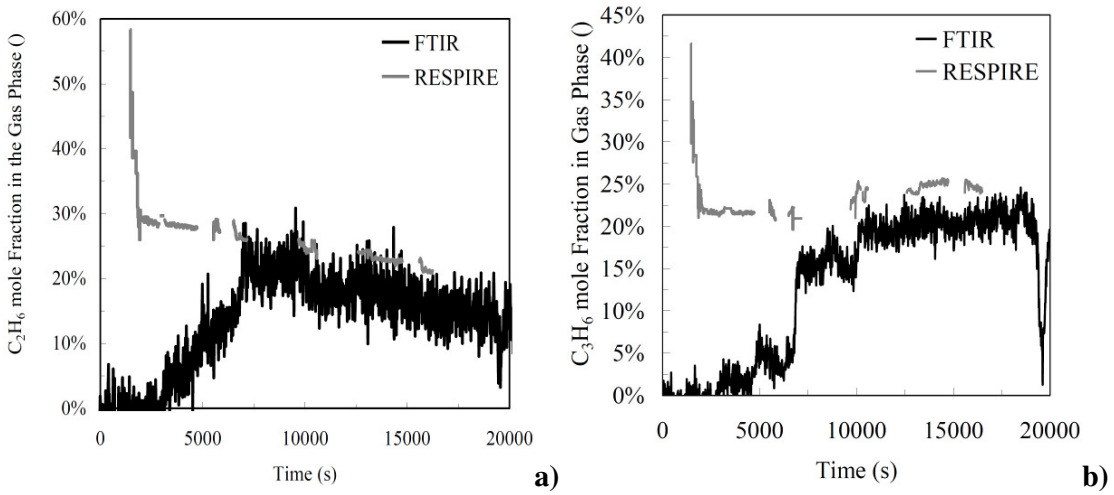

Figure 3. Measured and computed ethane (a) and propylene (b) mole fractions as a function of time.

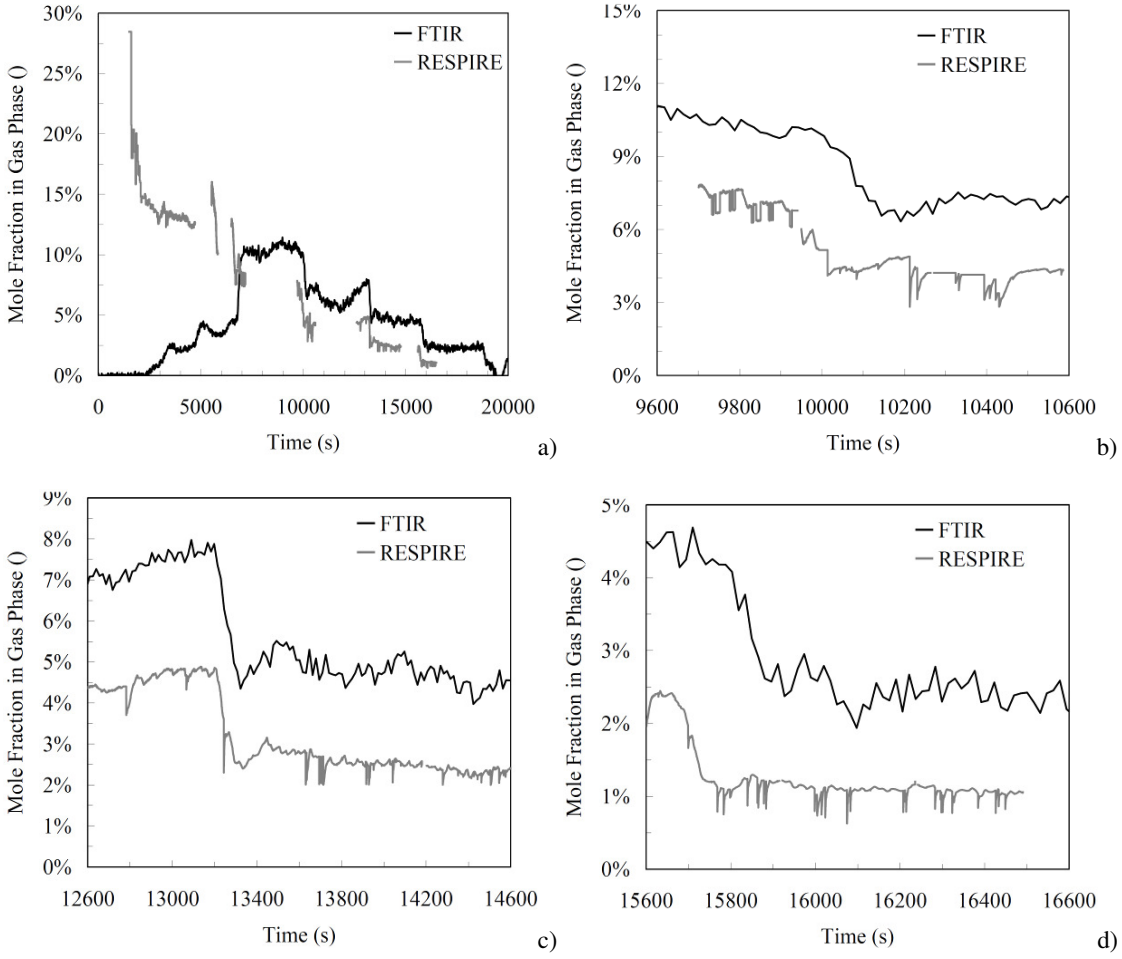

Figure 4. Measured and computed propane mole fractions as a function of time (a) with zoom in around 10100 s (b), 13600 s (c) and 16100 s (d).

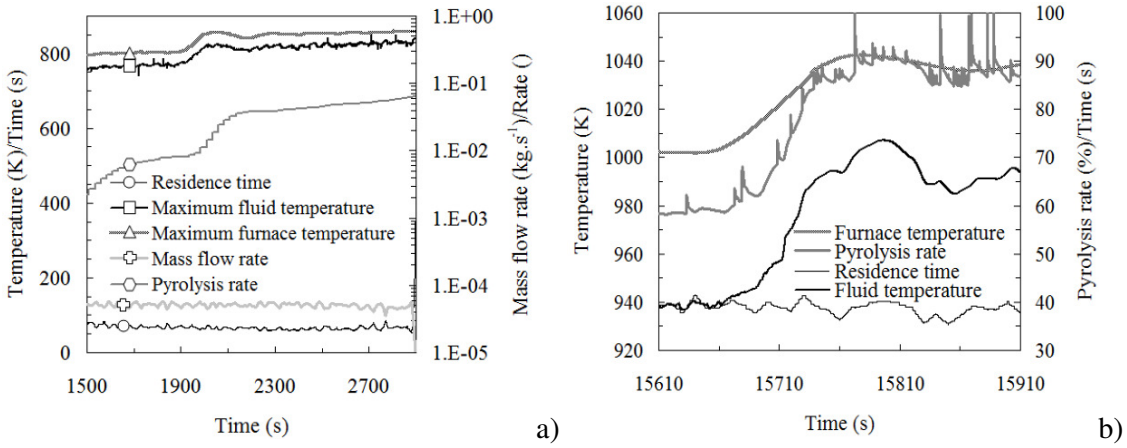

Figure 5. Numerical results of the dynamics of observed physical and chemical parameters for low (a) and high (b) gasification during temperature increase (dodecane pyrolysis, 10 bar, 0.05 g.s^{-1}, Ti reactor).

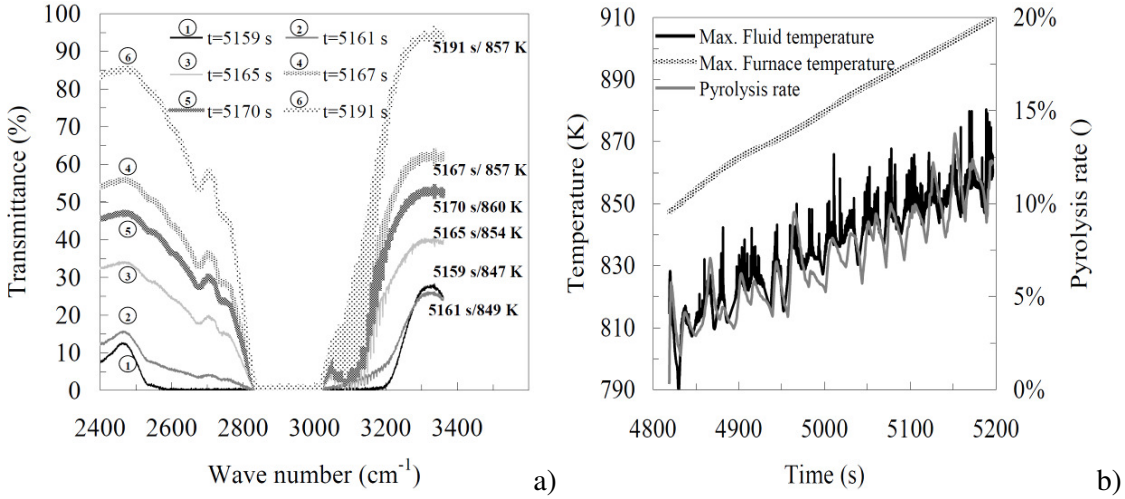

Figure 6. Modification of the measured IR in situ signal during the dodecane pyrolysis for several time steps and corresponding numerical fluid temperature (a) and associated numerically computed thermal and chemical data (b).

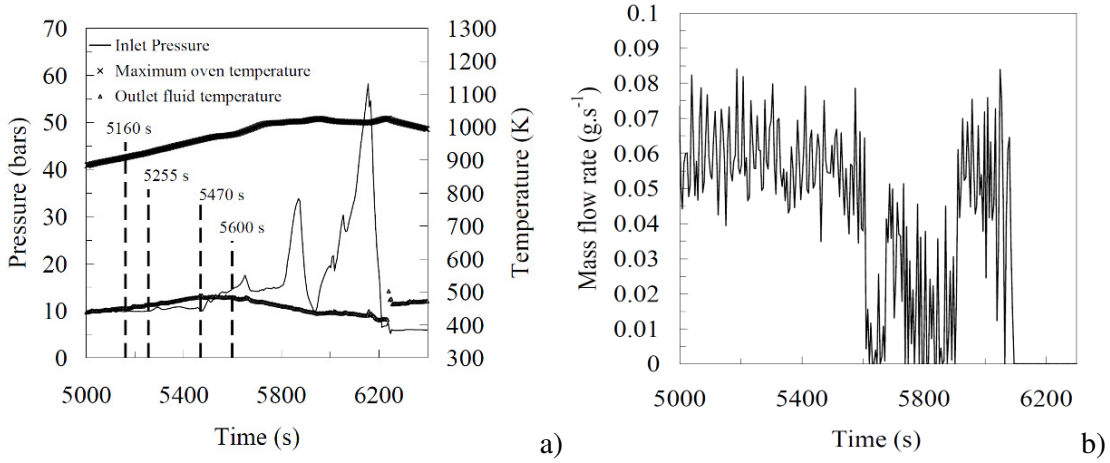

Figure 7. Pressure and temperature measured during the transient thermal increase (a) and related mass flow rate (b).

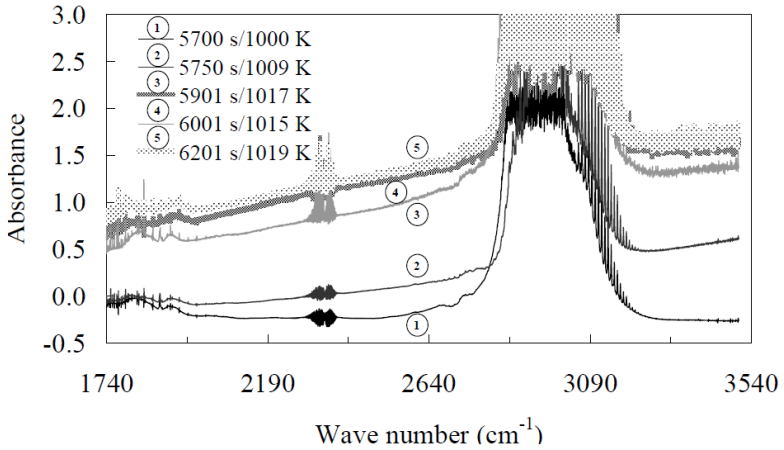

Figure 8. Coking activity detected by FTIR measurement.

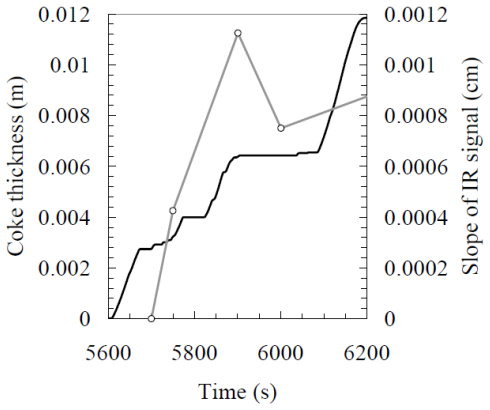

Figure 9. Qualitative comparison of the measured FTIR signal tilt with the computed coke thickness.

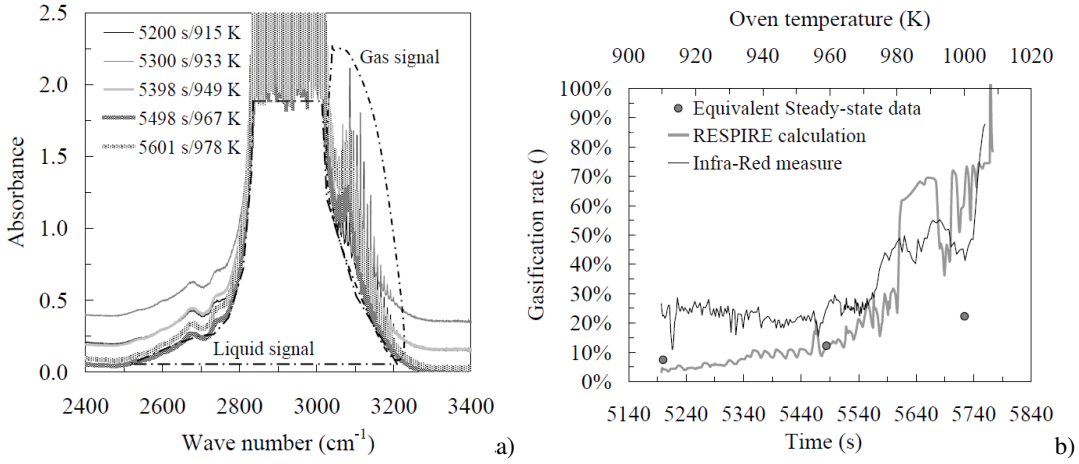

Figure 10. IR signal for several time steps with identification of liquid and gas signals (a) and associated quantification by ratio of corresponding surfaces as a function of experimental time and of oven temperature (b).

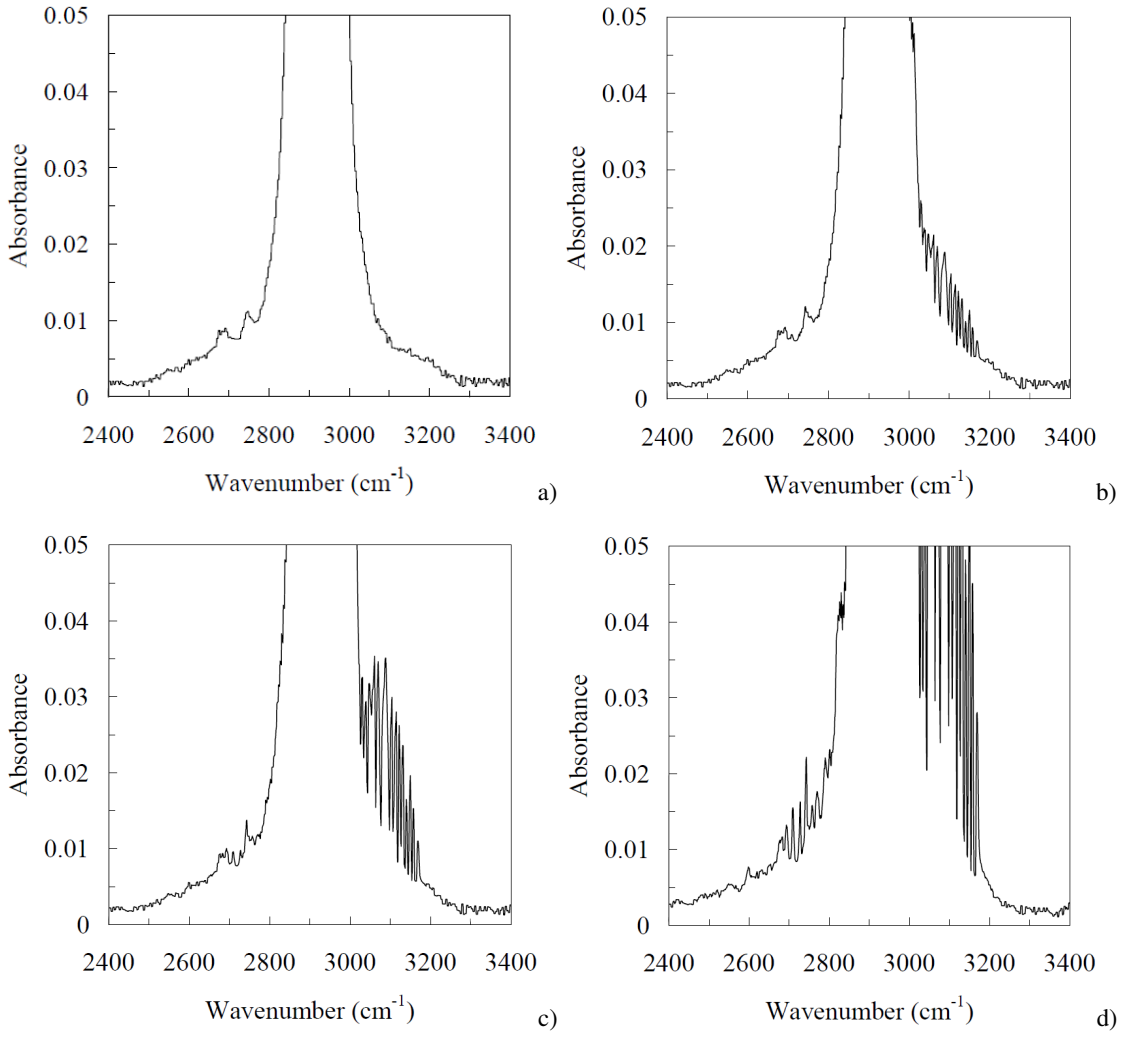

Figure 11. Qualitative numerical estimation of IR signals for several dodecane/methane "mixtures" with different methane content: 0 mol.% (a), 2 mol.% (b), 5 mol.% (c), 20 mol.% (d).